ELSEVIER

International Journal of Fatigue 24 (2002) 1047–1062

International Journal of Fatigue

www.elsevier.com/locate/ijfatigue

Mixed-mode, high-cycle fatigue-crack growth thresholds in Ti–6Al–4V: Role of small cracks

R.K. Nalla [a], J.P. Campbell [b], R.O. Ritchie [a,*]

[a] *Department of Materials Science and Engineering, University of California, Berkeley, CA 94720-1760, USA*
[b] *Metals Fabrication Division, General Motors, Troy, MI 48084, USA*

Received 7 September 2001; received in revised form 19 December 2001; accepted 25 January 2002

Abstract

There have been few studies to date describing fatigue-crack propagation thresholds under mixed-mode loading conditions in the presence of cracks, that are small as compared to the characteristic microstructural dimensions. To address this need, the variation in mixed-mode, high-cycle fatigue-crack growth thresholds with crack size is reported for a Ti-6Al-4V turbine blade alloy with a fine-grained bimodal microstructure. Specifically, threshold behavior is examined for large through-thickness cracks >4 mm in length), short through-thickness cracks (~200 μm in length), and microstructurally-small surface cracks (10–50 μm in diameter) under combined mode I and mode II loading at load ratios (ratio of minimum to maximum load) ranging from 0.1 to 0.8. For mode-mixities ranging from pure mode I to predominantly mode II, large crack, mode I $\Delta K_{I,TH}$ thresholds were found to decrease substantially with increasing phase angle. However, by characterizing in terms of the range in strain energy release rate, ΔG_{TH}, incorporating both mode I and mode II contributions, it was observed that the pure mode I threshold could be regarded as a 'worst case' under mixed-mode loading in this alloy. By estimating the effective crack-driving force actually experienced at the crack tip, the observed increase in the mixed-mode ΔG_{TH} threshold with mode-mixity was attributed to an increasing influence of crack-tip shielding due to crack closure and crack-surface interference. Equivalent thresholds for through-thickness short cracks, where the crack wake and hence the effect of such shielding is minimized, were consequently far less sensitive to mode-mixity and corresponded in magnitude to the shielding-corrected large-crack thresholds. This effect was accentuated for the measured thresholds of microstructurally-small surface cracks; such small-crack, mixed-mode ΔG_{TH} thresholds not only displayed a minimal influence of mode-mixity but were up to two orders of magnitude smaller than those for corresponding large cracks at the same load ratio and mode-mixity conditions.

Keywords: High-cycle fatigue; Mixed mode; Fatigue thresholds; Load ratio effects; Small crack effects; Crack-tip shielding; Ti–6Al–4V; Titanium

1. Introduction

The occurrence and control of failures due to high-cycle fatigue (HCF) in turbine engine components is currently one of the most critical challenges facing the US military aircraft fleet; in fact, a large fraction of recent engine failures have been attributed to HCF [1–3]. One particular issue involved in this problem is the prediction of the limiting conditions for HCF failures in the presence of multiaxial stresses; this can occur, for example, at sites of fretting fatigue in the turbine blade dovetail/disk contact section [4]. Although the driving force for cracks in these situations is a combination of tensile (mode I), in-plane shear (mode II) and/or anti-plane shear (mode III) loading, the vast majority of research on fatigue-crack growth behavior in typical turbine blade alloys, such as Ti–6Al–4V, has been limited to pure mode I behavior (e.g. [5–9][1]). Despite this preponderance of mode I data, there has been an increasing awareness in recent years of the role of mode-mixity in influencing fatigue-crack growth behavior in metallic materials (e.g. [11-18]), with a handful of studies

* Corresponding author. Tel.: +1-510-486-5798; fax: +1-510-486-4881.
E-mail address: roritchie@lbl.gov (R.O. Ritchie).

[1] It is interesting to note in this regard that although fatigue failure in materials has been documented for over a century, the first investigations on multiaxial fatigue occurred only as recently as 1969 [10].

0142-1123/02/$ - see front matter
PII: S0142-1123(02)00020-8

devoted to Ti–6Al–4V (e.g. [16-18]). However, few investigations have focused on the role of crack size in influencing fatigue-crack growth behavior under multiaxial conditions, and specifically on how the presence of microstructurally-small cracks may affect mixed-mode fatigue thresholds. The present work seeks to address this problem for the high-cycle fatigue of turbine blade materials, specifically for a Ti–6Al–4V alloy with a bimodal microstructure.

2. Background

The HCF problem in turbine engine components is associated with a variety of drivers [3], which vary with component and indeed location on that component (Fig. 1). Typically, these components, such as blades and disks, are subjected to high frequency (> 1 kHz) vibrations in the engine (HCF), superimposed on to a low-cycle fatigue component associated with the start-to-stop cycles [2,3]. A critical site for crack initiation is in the attachment section of the blade, where contact between the blade dovetail and disk leads to the formation of fretting fatigue cracks [4]. This problem often involves complex multiaxial loading conditions, surface damage, and associated residual stresses.

At present, most design and 'lifing' methodologies for HCF use traditional stress-life (*S–N*) and Goodman diagram approaches. However, in light of the high frequencies involved, once a fatigue crack starts propagating, final failure can ensue rapidly; consequently, alternative fracture-mechanics based design methodologies utilizing the concept of a threshold stress-intensity, below which no fatigue-crack growth is observed, may offer a preferred approach, provided such thresholds are defined under representative HCF conditions. Unfortunately, as noted above, most available fatigue threshold data (e.g. [19]) have been measured in tension (mode I) on through-thickness cracks, large compared to the microstructural size-scales. These are conditions that may not be relevant to turbine engine HCF, where the loading can be mixed-mode and crack sizes can be of the order of a fraction of a millimeter. In terms of defining a conservative HCF threshold, both these factors are important as small cracks are known to grow (at least in mode I) at apparently anomalously high velocities, well below the established large-crack propagation thresholds [20]; similarly, the superposition of shear loading (resulting in finite mode II or III stress-intensity ranges, ΔK_{II} and ΔK_{III}, respectively, at the crack tip) has been shown to cause a substantial reduction in the mode I fatigue threshold, $\Delta K_{I,TH}$, below which the crack growth is presumed to be dormant (e.g. [10,13,14,16,17]).

Our previous studies [21] on this alloy have shown such a reduction in the $\Delta K_{I,TH}$ threshold with increasing mode-mixity, although the majority of this work was devoted to large (>4 mm) through-thickness cracks. Furthermore, the variation in threshold behavior with mode-mixity was found to be related to the degree of crack-tip shielding, by mode I crack closure and mode II crack-surface interference [21,22], which acts locally to reduce the effective driving force at the crack tip [22]. As the potency of such shielding is substantially reduced for cracks with limited wake (e.g. [23-26]), it is important to assess the role of mode-mixity in influencing fatigue threshold behavior for small cracks, where cracks are of a size comparable to the scale of microstructure ahead of the crack tip and/or the extent of shielding behind it. In addition, it is critical to distinguish between these two effects, by comparing the behavior of short cracks that are small only in the length dimension (which limits shielding) with those that are small in all dimensions (which limits both shielding and the ability to 'sample' the continuum microstructure).

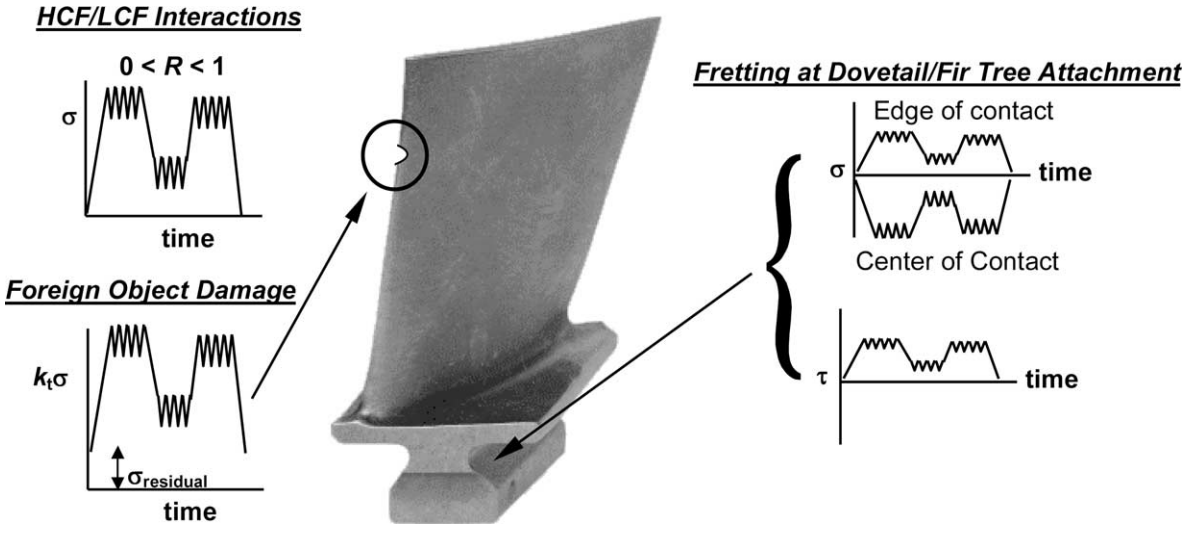

Fig. 1. Diagram illustrating the variety and range of factors involved in HCF failure.

Table 1
Chemical composition of Ti-6Al-4V bar stock (in wt%) [28]

Bar location	Ti	Al	V	Fe	O	N	H
Top	Bal.	6.27	4.19	0.20	0.18	0.012	0.0041
Bottom	Bal.	6.32	4.15	0.18	0.19	0.014	0.0041

Accordingly, in the present work we examine the role of crack size through a study of the mixed-mode, fatigue-crack growth thresholds in Ti–6Al–4V for large (>4 mm), short (~200 μm) and microstructurally-small (<50 μm) cracks[2], over a range of mode-mixities from pure tension ($\Delta K_{II}/\Delta K_I = 0$) to predominantly shear ($\Delta K_{II}/\Delta K_I \sim 7.1$), at positive load ratios (ratio of minimum to maximum load) between $R = 0.1$–0.8.

3. Experimental procedures

3.1. Materials

The material investigated, a turbine engine Ti–6Al–4V alloy, originated as bar stock produced by Teledyne Titanium specifically for the joint government–industry–academia HCF program; its composition (in wt.%) is given in Table 1. The original bar-stock (63.5 mm in diameter) was sectioned into segments 400 mm long, preheated to 940°C for 30 min and forged into $400 \times 150 \times 20$ mm plates. These plates were solution-treated at 925°C for 1 h, fan air cooled and then stabilized at 700°C for 2 h. The microstructure of this alloy was examined in the as-received, bimodal condition (sometimes referred to as solution treated and over-aged—STOA), consisting of colonies of equiaxed primary-α and lamellar α+β (transformed-β) (Fig. 2). A careful investigation of the relative distribution of the two phases indicated an overall primary-α content of ~64% [27]. The average grain size obtained was ~20 μm, with slight grain elongation observed in the longitudinal (L) direction of the forging. Using differential thermal analysis, the β-transus temperature was measured to be 990–1005 °C.

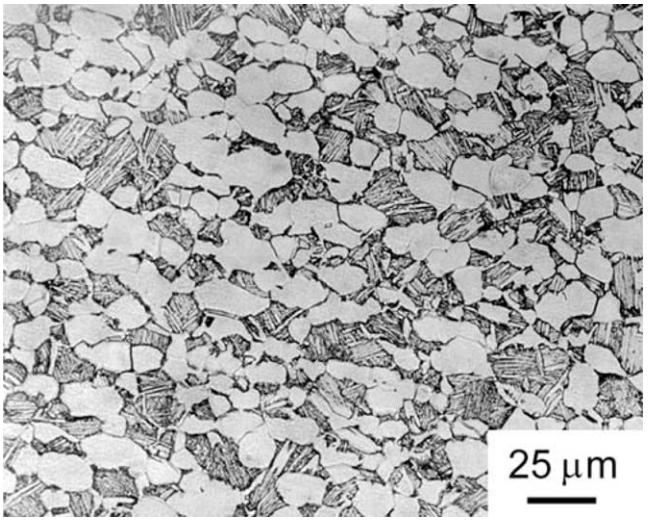

Fig. 2. Optical micrograph of the bimodal (solution treated and over-aged, STOA) Ti–6Al–4V microstructure investigated. Etched for ~10 s in 5 parts 70% HNO_3, 10 parts 50% HF, 85 parts of H_2O.

[2] The distinction between large, short and small cracks is described in Appendix A.

3.2. Uniaxial tensile and toughness properties

Uniaxial tensile tests were conducted in the L-orientation using a strain rate of 5×10^{-4} s^{-1}; additional data were taken from [28]. The yield and tensile strengths for this microstructure were found to be 930 and 978 MPa, respectively, with a reduction in area of ~45%. In addition, the plane-strain fracture toughness, K_{Ic}, was measured at 64 MPa√m, using ~18-mm thick, fatigue-precracked, compact-tension samples.

3.3. Large-crack fatigue testing

Fatigue thresholds in pure mode I were conducted using 4.5-mm thick, 11.3-mm wide symmetric four-point bending samples, with inner and outer loading spans of 12.7 and 25.4 mm, respectively. For mixed-mode loading, the mode II component of the loading was introduced using the asymmetric four-point bending (AFPB) configuration, where the $\Delta K_{II}/\Delta K_I$ ratio can be varied using an offset, s, from the load-line as shown in Fig. 3(a) (e.g. [13,29]). The values of mode I stress-intensity range, ΔK_I, and the mode II stress-intensity range, ΔK_{II}, were determined from linear-elastic stress-intensity solutions for this geometry, recently developed by He and Hutchinson [30].

Since mixed-mode thresholds were determined from the initiation, rather than the arrest, of crack growth from a precrack, the process of precracking itself was conducted in a carefully-controlled, near-identical manner for all large-crack test samples to minimize any effects of this procedure on the subsequent threshold determination. Specifically, fatigue cracks were grown in room air from a 2 mm deep electro-deposition machined (EDM) through-thickness notch in a symmetric four-point bending sample at a load ratio, R of 0.1 with a

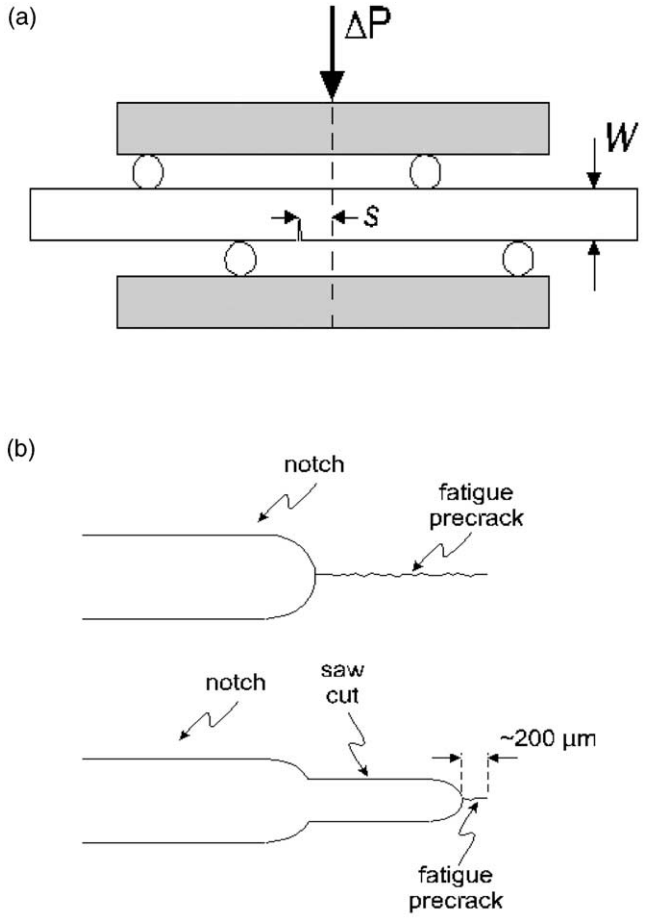

Fig. 3. (a) The asymmetric four-point bend specimen. The offset *s*, from the load-line is used to control the degree of mode-mixity, $\Delta K_{II}/\Delta K_I$, and thereby the phase angle, $ß = \tan^{-1}(\Delta K_{II}/\Delta K_I)$. (b) The procedure used to remove the crack wake of a large crack in order to produce a short crack is illustrated.

constant loading frequency (125 Hz, sine wave). This alloy has been known to show little effect of frequency over the range 50–20,000 Hz [8,31]. In all samples, the final precrack length achieved was 4.50±0.25 mm at a near-threshold stress-intensity ΔK of 4.8±0.5 MPa$\sqrt{m}$.

For large crack (> 4 mm) tests, mode-mixities varied from $\Delta K_{II}/\Delta K_I = 0$ (pure mode I) to ~7.1 (nearly pure mode II), representing a change in phase angle, $\beta = \tan^{-1}(\Delta K_{II}/\Delta K_I)$, from 0 to 82°. Load ratios were varied from $R = 0.1$ to 0.8. Tests involving cycling pre-cracked specimens at a specified mode-mixity were performed in the following way: if no crack growth was observed (using an optical microscope) after 2×10^6 cycles, either ΔK_I or ΔK_{II} was increased by ~0.25 MPa$\sqrt{m}$ and the procedure repeated. In this way, a 'growth/no growth' condition bounding the actual threshold was obtained. The crack extension defining 'growth' was taken to be of the order of the characteristic microstructural dimension, i.e., ~20 μm, yielding threshold growth rates of 10^{-11} m/cycle.

The magnitude of the crack-tip shielding, used to compute the effective crack-driving force in both modes I and II, was characterized using a recently developed compliance-based technique for both tensile opening and shear type loading, using two displacement gauges mounted near the crack tip to measure opening and shear displacements. As described in detail in [22], the distinction between the contributions to shielding in modes I and II was achieved by examining separate load-displacement curves using these two crack-tip gauges. Mode I shielding, in the form of crack closure, was determined from the compliance curve for the opening displacements from the first deviation from linearity on unloading, whereas mode II shielding, in the form of asperity rubbing and interlock, was determined in an analogous fashion from the compliance curve for shear displacements.

3.4. Short-crack fatigue testing

For corresponding tests on short cracks, thresholds were measured using identical procedures on 6–12 mm thick bend bars, except that the precrack wake was the carefully machined to within ~200 μm of the crack tip using a slow-speed, 0.3-mm thick, diamond saw (Fig. 3(b)). The rationale here was to limit the shielding (due to premature contact of the crack faces during unloading) by restricting the crack wake, without affecting the degree of sampling of the microstructure along the crack front (as described in the Appendix A). As for large cracks, thresholds were obtained at load ratios ranging from $R = 0.1$ to 0.8 for mode-mixities of $\Delta K_{II}/\Delta K_I = 0$ to ~7.1.

The removal of the precrack wake left a machined notch with a measured (semi-circular) root radius of $\rho \approx 160$ μm, ~200 μm from the tip of the short crack (Fig. 3b). This, however, was reasoned to not affect the stress and strain field of the short crack. According to Dowling's analysis of the stress intensity for a short crack, of length *l*, emanating from a notch [32], the elastic notch field is felt over a distance of 0.1–0.2 l/ρ from the notch surface, i.e., over a distance of <40 μm, far less than the length of the short crack. The corresponding plastic field of the notch can be estimated from the Neuber analysis of Hammouda et al. [33], which gives the extent of bulk plasticity as a simple function of the stress level, yield strength and notch size and shape. For the present experiments, this analysis gave a notch plastic field of ~20 μm, which is again far less than the length of the short crack. Finally, using Rice and Johnson's analysis of a blunted crack tip [34], based on Hill's logarithmic spiral slip-line field solution for a rounded notch [35], the maximum stress of the notch plastic field peaks at a distance of 0.95ρ i.e., in the present case ~150 μm, from the notch tip, which again implies that the tip of the short crack is well outside the influence of the notch.

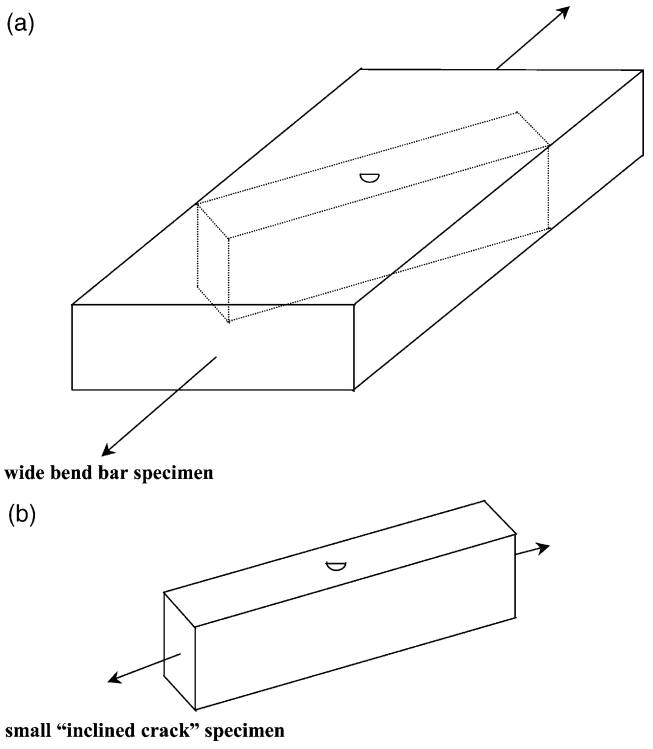

Fig. 4. A schematic illustration showing the procedure utilized for obtaining the small 'inclined crack' specimen. (a) The dotted lines outline the small crack test sample to be machined at the desired angle of inclination, ϕ (see Fig. 5) from the original wide bend bar. The nominal direction of loading for crack initiation is also shown. (b) The final 'inclined crack' specimen is illustrated.

3.5. Small-crack fatigue testing

Corresponding mixed-mode testing on microstructurally small cracks was performed using an inclined crack method. Specifically, small, semi-elliptical, surface 'precracks' were naturally initiated on wide, three-point bend samples (5 mm thick, 16–25 mm wide, with a span of 25.4 mm) machined in the L–T orientation (Fig. 4), at a maximum stress of $\sigma_{max} \sim 750$ MPa (~80% of yield strength) at 50 Hz sinusoidal frequency with $R = 0.1$. The surfaces necessary for observation of the crack were polished to a 0.05 μm finish, with the sides to be used to carry the load-bearing pins ground to a 600 grit finish. Following specimen preparation, a stress relief treatment of 2 h at ~695°C in vacuo was used to minimize residual stresses.

In order to measure a mixed-mode, small-crack thresholds, smaller bend bars were carefully machined out from the original pre-cracked bar with the crack inclined at the desired angle, ϕ, to the length of the sample (Figs. 4–5). The smaller bend bars containing the inclined small surface cracks were then used for threshold determination by cycling in symmetric four-point bending with a load ratio of 0.1. Similar to large and short-crack testing, thresholds were determined using a 'growth/no growth' criterion. Specifically, if no growth, defined as

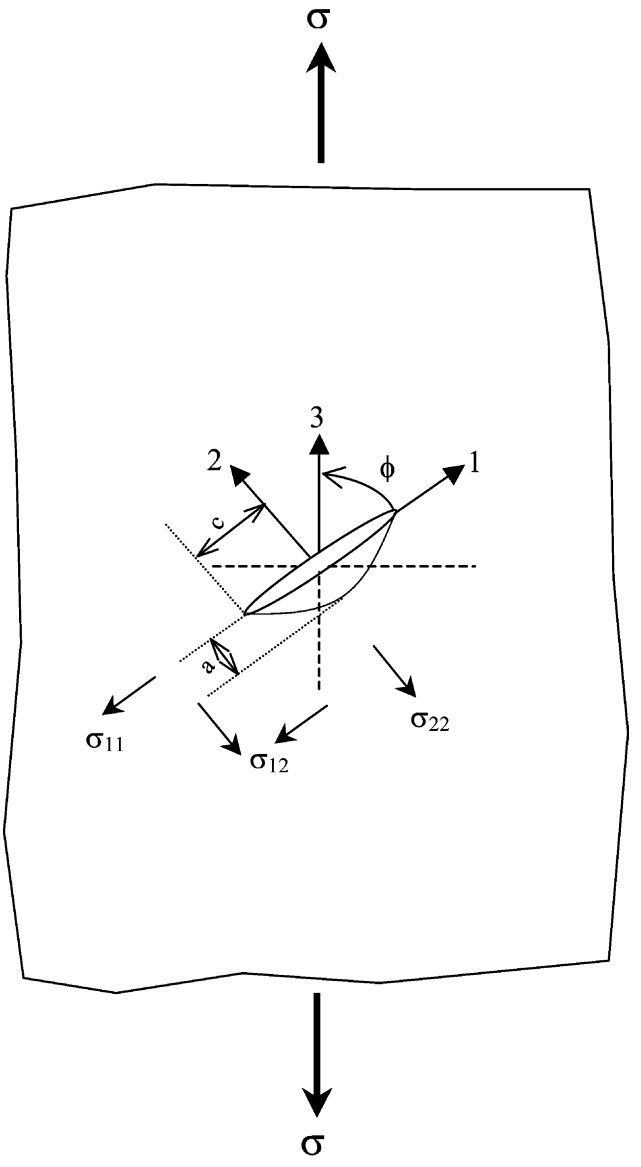

Fig. 5. A schematic of the inclined semi-elliptical surface crack configuration used for the microstructurally-small crack testing. The crack depth, a, and the crack (half) size, c, are indicated, as is the angle of inclination, ϕ. The tensile loading component, σ_{22} induces the mode I contribution, while the shear loading component, σ_{12} induces the mode II and mode III components. σ_{11} has no influence.

a total of 20 μm per 2×10^6 cycles on both ends of the surface crack was observed, the maximum load (and in proportion the minimum load) was increased by 111 N and the procedure repeated.

Linear-elastic solutions for the stress intensities associated with the small, semi-elliptical surface cracks under mixed-mode loading were taken from two sources. On the basis that the crack plane was normal to the specimen surface, the mode I component of the stress intensity, K_I, was computed from the well-known Newman–Raju solution [36]:

$$K_{\mathrm{I}} = (\sigma_t + H\sigma_b)\sqrt{\pi\frac{a}{Q}}\,F\left(\frac{a}{t}, \frac{a}{c}, \frac{c}{b}, \theta\right)$$

where σ_t is the remote uniform-tension stress and σ_b is the remote uniform outer-fiber bending stress. The geometrical factors H, Q and F are evaluated from the crack depth, a, the crack half-length, c, the specimen thickness, t, the specimen half-width, b, and the angular position along the crack front, θ, as described in detail in [36].

The mode II component, K_{II}, conversely, was computed from the newly derived He-Hutchinson solution [37] for elliptical surface cracks under mixed-mode loading:

$$K_{\mathrm{II}} = \chi\sigma_{12}\sqrt{\pi a}$$

where χ is a numerical factor determined using ref. [37], σ_{12} is the shear component of the loading (see Fig. 5) and a is the crack depth. It should be noted here that a three-dimensional corner singularity exists in the solution at the point where the crack intersects the free surface; however, for the purpose of this study, this is ignored since errors caused by such an assumption are negligible. Moreover, as one moves along the crack front to the interior, the magnitude of the mode II contribution decreases, with that of mode III increasing till the point of deepest penetration of the crack is reached.

The applied load/stress on the inclined crack (Fig. 5) was resolved trigonometrically into tensile and shear components. The tensile component was used for determining ΔK_{I}, using [36], and the shear component for ΔK_{II} and ΔK_{III}, using [37]. As the exact shape of such small surface cracks and the variation in the aspect ratio with crack extension clearly can have an important effect on the crack driving force and hence the crack-growth behavior [38,39], crack shapes (Fig. 5), in the form of the depth to surface length ratio, $a/2c$, were determined by breaking open the sample after testing; typical aspect ratios were in the range of $a/2c$~0.45.

The use of linear-elastic stress-intensity solutions for characterizing the driving forces for the small cracks is justified on the basis of the small cyclic plastic-zones sizes in relation to crack size. For example, for the smallest crack sizes of ~1 μm, where the ΔK_{I} thresholds are ~1 MPa√m, plastic-zone size (estimated as r_{y} ~$1/2\pi(\Delta K_{\mathrm{I}}/\sigma_{\mathrm{y}})^2$ where σ_{y} is the yield strength) are on the order of 100 nm. As this is roughly one tenth of the crack size, it is deemed reasonable to conclude that small-scale yielding conditions prevail.

4. Results and discussion

4.1. Large-crack behavior

4.1.1. Effect of load ratio and mode-mixity

Results indicating the large-crack threshold behavior under mode I+II loading are shown in Fig. 6 in the form of mixed-mode threshold envelopes, where the mode II threshold stress-intensity range, $\Delta K_{\mathrm{II,TH}}$, is plotted as a function of the corresponding mode I threshold stress-intensity range, $\Delta K_{\mathrm{I,TH}}$. The threshold envelope is shown along with the corresponding bounding 'growth' (open symbols) and 'no growth' (closed symbols) conditions for load ratios of 0.1, 0.5 and 0.8 at mode-mixities ranging from pure mode I, i.e., $\Delta K_{\mathrm{II}}/\Delta K_{\mathrm{I}} = 0$ (phase angle, $\beta = 0°$), to nearly pure mode II, i.e., $\Delta K_{\mathrm{II}}/\Delta K_{\mathrm{I}}$ ~ 7.1 ($\beta = 82°$). Similar to behavior in other materials [13,14], a clear reduction in mode I $\Delta K_{\mathrm{I,TH}}$ threshold values is evident with increasing load ratio. Moreover, the value of $\Delta K_{\mathrm{I,TH}}$ can also be seen to generally decrease with increasing phase angle (except for a slight increase at low phase angles between 0 and 26°, which has been attributed to an effect of mode I/mode II crack-tip shielding [22]).

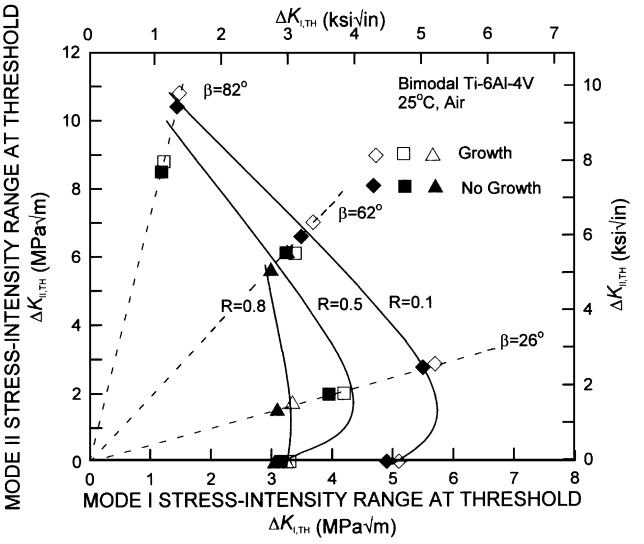

Fig. 6. Mixed-mode threshold envelopes for the bimodal microstructure. Note the deterioration of mixed-mode fatigue resistance with increasing load ratio.

4.1.2. Single parameter characterization

Although the mode I threshold, $\Delta K_{\mathrm{I,TH}}$, clearly decreases with increasing mode-mixity, if a more appropriate measure of the mixed-mode driving force is used, specifically the range in strain-energy release rate, $\Delta G = (\Delta K_{\mathrm{I}}^2 + \Delta K_{\mathrm{II}}^2)/E'$, where $E' = E$ (Young's modulus) in plane stress and $E/(1-\nu^2)$ in plane strain (ν is Poisson's ratio),[3] then there is a progressive increase in the mixed-mode threshold, ΔG_{TH}, with increasing

[3] Note that with the definition used, ΔG does not necessarily equal $G_{\max}$–$G_{\min}$, where $G_{\max}$ and $G_{\min}$ are determined from the maximum and minimum loads of the fatigue cycle. Alternatively, mixed-mode crack-growth and threshold data can be represented in terms of an equivalent stress-intensity range, given by $\Delta K_{\mathrm{eq,TH}} = (\Delta G_{\mathrm{TH}} E')^{1/2}$.

mode-mixity at all load ratios studied (Fig. 7).[4] This marked effect of increasing mode-mixity is such that the ΔG_{TH} threshold at $\beta = 82°$ is some 4–5 times larger than the mode I value ($\beta = 0°$) at $R = 0.1$. From the perspective of thresholds for high-cycle fatigue, this implies that in terms of mixed-mode loading, the mode I threshold, defined in terms of ΔG, represents a *worst-case* condition; similar observations have been made in other material systems [40,41]. Consequently, the presence of mixed-mode conditions does not preclude the use of a threshold-based design methodology for high-cycle fatigue.

An alternative means of calculating the mixed-mode threshold, which accounts for the deflection of the crack once propagation ensues, is described in Appendix B. This leads to a small change, generally a reduction, in the value of ΔG_{TH}.

4.1.3. Crack path and fractographic observations

A typical crack path for through-thickness large cracks is illustrated in Fig. 8(a). This profile shows the mode I fatigue pre-crack (at $R = 0.1$) and the crack path following the application of mixed-mode loading conditions at $R = 0.8$ with $\beta = 26°$ ($\Delta K_{II}/\Delta K_I = 0.5$). It is apparent that unlike behavior in a coarser lamellar microstructure in this alloy [42], the crack path in the finer-scale bimodal condition is not markedly influenced

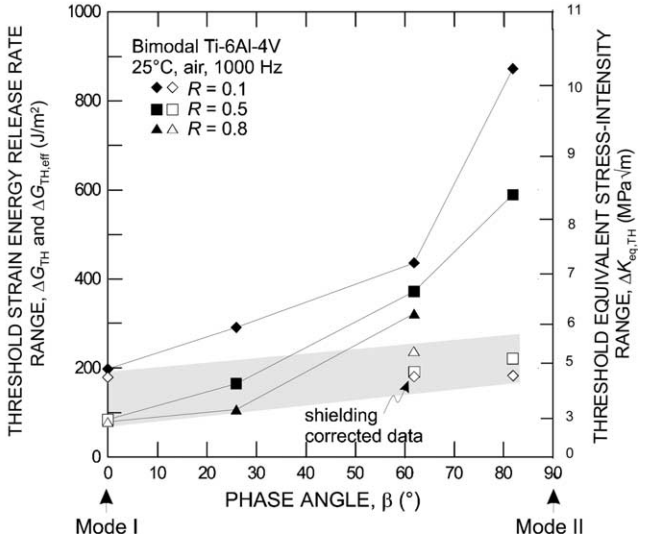

Fig. 7. The threshold strain-energy release rate, ΔG_{TH} is given as a function of phase angle, β for large through-thickness cracks. Equivalent stress-intensity factor ranges at threshold, $\Delta K_{eq,TH}$ are also shown. The mode I threshold clearly represents a *worst-case* condition. Correction for shielding using the recently developed compliance based technique is also shown. Note the relative absence of any effect of mode-mixity and/or load ratio on the shielding-corrected thresholds (after [22]).

[4] Threshold values plotted in Fig. 7 represent the average of the 'growth' and 'no growth' conditions from Fig. 6.

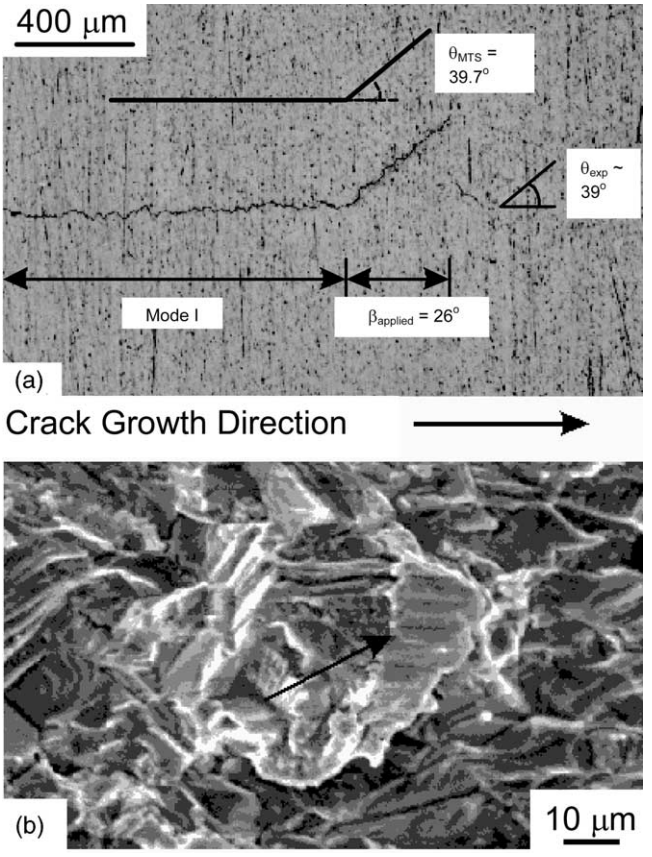

Fig. 8. (a) Fatigue crack profiles are compared for the bimodal ($R = 0.8, \beta = 26°$) microstructure. Optical micrographs show both the mode I fatigue pre-crack and the region of deflected crack growth following the application of cyclic mixed-mode loading. Measured crack deflection angles, θ_{exp}, are compared with those predicted by the path of maximum tangential stress, θ_{MTS}, and (b) Corresponding fractography of the near-tip crack wake showing evidence of fracture surface abrasion (indicated by arrow), presumably due to shear-induced fracture surface contact (from [22]). The ΔG levels involved were ~85 J/m^2.

by microstructure. Specifically, the crack path (for both mode I and mixed-mode loading) is relatively planar with a degree of tortuosity only on the order of the characteristic microstructural size-scales (~20 μm).

Crack paths result from the mutual interaction of the maximum crack-driving force and the weakest microstructural path. In a fine-scale, homogeneous structure such as the bimodal Ti–6Al–4V where the microstructural considerations are of secondary importance, the path of a growing fatigue crack will change primarily in response to a change in the applied phase angle, the most likely criterion for the crack trajectory being that a purely mode I condition at the crack tip, such that the crack will follow a path dictated by the maximum tangential stress, $K_{II} = 0$, or maximum G [15,42–44]. Except for small differences at very high phase angles, these criteria yield essentially the same crack-path predictions.

In Fig. 8(a), it can be seen that after the application

of the mixed-mode loading, the crack proceeds along a direction that is virtually identical to that dictated by a criterion of maximum tangential stress (MTS) [15,43,44]; i.e., it propagates in mode I. More detailed discussion of the effect of mode-mixity on crack path can be found in [21,44].

Fractographically, fatigue fracture surfaces were similar for crack growth under pure mode I and mixed-mode loading. However, there was one distinct difference in that there was evidence of abrasion on the fracture surfaces for growth under mixed-mode loading (Fig. 8(b)). This is to be expected due to the relative shear displacements of the crack surfaces under mixed-mode loads; moreover, such evidence is an indication of the occurrence of crack-surface interference during mixed-mode crack growth.

4.1.4. Shielding-correction for large-crack thresholds

It is well established that under mixed-mode loading, there is a potential for such interference between the sliding crack surfaces (e.g. [22,45,46]); indeed, the friction and rubbing between the surfaces represents a potent form of crack-tip shielding [45–50], akin to crack closure in mode I (e.g. [51,52]. As discussed in detail elsewhere [21,22], the increase in the large-crack, mixed-mode ΔG_{TH} threshold with increasing mode-mixity in this microstructure (shown in Fig. 7) can be related to an increased role in such mode I and mode II shielding, associated, respectively, with crack closure and sliding crack interference from the friction and interlock of crack-surface asperities. Indeed, the magnitude of such shielding can be quantified using compliance-based techniques [22]. This was performed using both mode I opening and mode II side-mounted crack-tip displacement gauges to measure the effective (near-tip) stress intensities in modes I and II. In this manner, the ΔG_{TH} threshold data were 'corrected' for the presence of shielding by characterizing the driving force in terms of a mixed-mode, effective threshold strain-energy release rate, $\Delta G_{TH,eff}$. Results are illustrated in Fig. 7 [22]. It is apparent that once the effect of closure and crack-surface interference are removed, the effects of mode-mixity and load ratio on the fatigue threshold are both greatly reduced. Moreover, 'correcting' the driving force for mixed-mode shielding can reduce the value of the large-crack ΔG_{TH} thresholds by up to almost an order of magnitude; specifically, whereas the ΔG_{TH} threshold in near-mode II ($\beta = 82°$) is some seven times its value in mode I, the corresponding difference in $\Delta G_{TH,eff}$ thresholds is less than a factor of 3.

These results strongly imply that the primary effect of increasing mode-mixity in increasing the value of the large-crack, mixed-mode ΔG_{TH} threshold can be attributed to an enhanced role of crack-tip shielding in modes I and II, which acts to diminish the effective driving force for crack growth. This is analogous to the well-known effect of decreasing load ratio in increasing the mode I threshold, which has similarly been largely attributed to (mode I) shielding (by crack closure) (e.g. [31,51]). These results also strongly suggest that short fatigue cracks will only show a minimal sensitivity to mode-mixity, as their limited wake acts to restrict such shielding; this question is discussed in detail below.

4.2. Short-crack behavior

Similar studies were performed on short cracks, approximately 200 μm in length, where the crack wake had been largely removed. Although such cracks still have dimensions that are large compared to microstructural size-scales (the crack front 'samples' several hundred grains), the limited wake acts to suppress the effect of any crack-tip shielding (e.g. [23,25]). Measured mixed-mode thresholds for such short cracks, expressed in terms of both ΔG_{TH} and $\Delta K_{eq,TH}$, are plotted in Fig. 9 as a function of the phase angle for load ratios of 0.1–0.8; results are compared with the corresponding thresholds for large cracks.

As alluded to above, the restricted role of wake shielding has a significant effect on the mixed-mode ΔG_{TH} thresholds for the short cracks. Specifically, short-crack thresholds can be seen to be:

- far smaller than large-crack values,
- relatively insensitive to mode-mixity,
- essentially insensitive to load ratio,
- comparable in magnitude to the shielding-corrected large-crack values.

Of particular note is that the substantial increase in the large-crack ΔG_{TH} thresholds at high mode-mixities

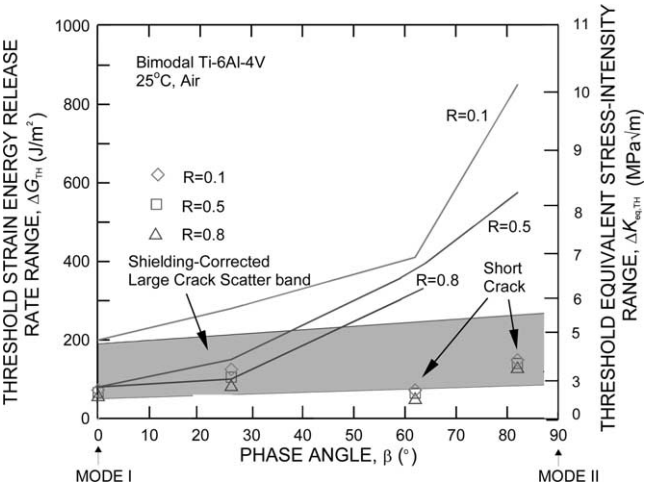

Fig. 9. Variation in mixed-mode thresholds, ΔG_{TH}, as a function of phase angle, β, in the bimodal structure. Shown are results at three load ratios for large (> 4 mm) cracks, before and after 'correcting' for crack-tip shielding, and for short (~200 μm) through-thickness cracks.

(β = 62°, 82°) is nearly eliminated for short cracks. These results clearly highlight the critical effect of crack size on mixed-mode fatigue-crack propagation behavior, in that when crack-tip shielding is accounted for, either by correcting the 'driving force' or limiting its magnitude by wake removal, the effect of mode-mixity on the ΔG_{TH} threshold behavior becomes relatively insignificant.

A typical crack profile (R = 0.1, β = 26°) and fractography (R = 0.1, β = 62°, ΔG ~72 J/m^2) are included in Fig. 10; the crack deflection angles agree very well with the MTS predictions. Identical to the large-crack results (Fig. 7), the extent of microstructurally-induced crack-path tortuosity was relatively minor, i.e., in the order of tens of micrometers, and the crack nominally followed a mode I path, as dictated by the MTS criterion following the application of the mixed-mode loading.

It is worth noting that the (through-thickness) short cracks investigated here had crack lengths roughly an order of magnitude larger than the average grain size, and widths over two order of magnitude larger; consequently, their crack fronts were presumed to 'sample' the microstructure adequately, akin to the large, through-thickness cracks discussed above. Such 'continuum sampling' would not be expected for cracks of true microstructural dimensions. Accordingly, we now examine the mixed-mode threshold behavior of small, semi-elliptical surface cracks, where all dimensions are comparable with microstructural size-scales.

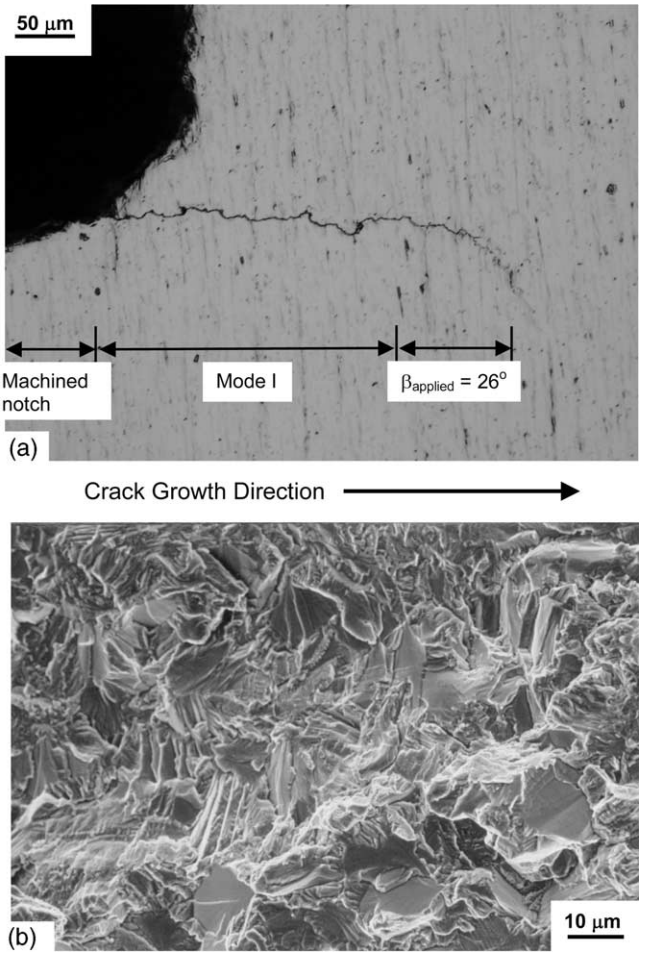

Fig. 10. (a) A typical crack profile (R = 0.1, β = 26°) obtained for through-thickness short (~200 μm) crack mixed-mode thresholds. (b) Near-tip mixed-mode fractography for specimen tested under R = 0.1, β = 62° (ΔG~72 J/m^2).

4.3. Microstructurally-small crack behavior

4.3.1. Small crack initiation and crack shape considerations

In the present study, small surface precracks were initiated naturally on wide three-point bend specimens.

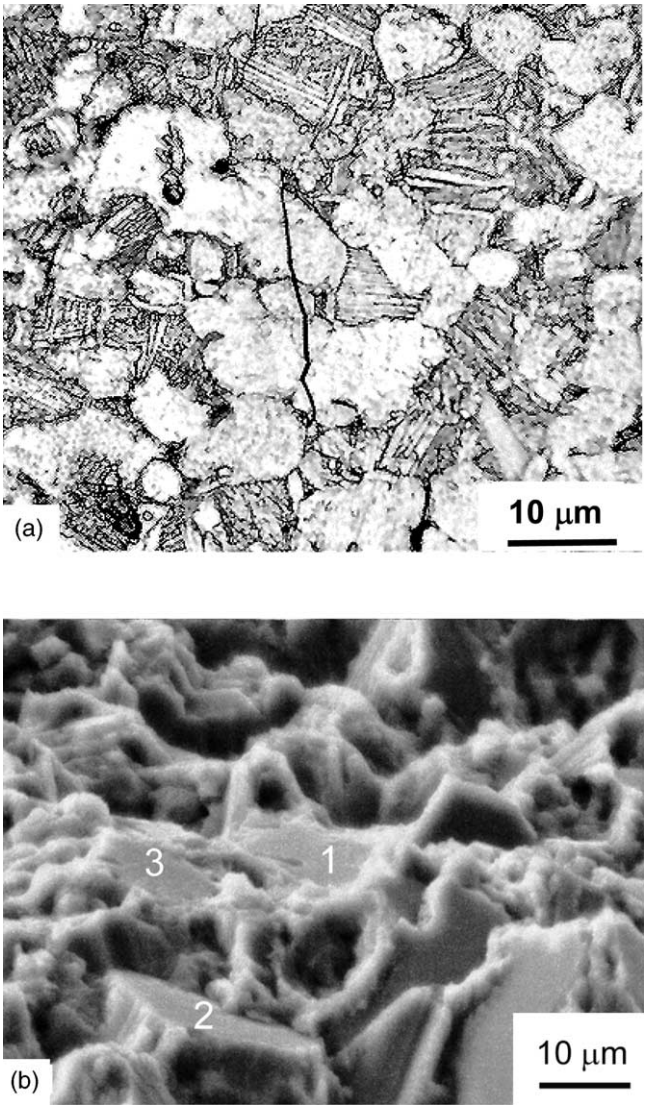

Fig. 11. (a) A typical fatigue-crack initiation site is illustrated for the bimodal microstructure in this optical photomicrograph. Note that initiation predominantly occurs in the primary-α grains, and (b) SEM image of crack initiation and early growth along planar slip bands leading to facet type fracture surface (specimen tilt: 70°). EBSD analysis of fractured α grains 1–3 revealed near-basal orientation of the fracture plane. [Fig. 11(b): Courtesy of Dr J.O. Peters].

Cracks were found to initiate preferentially within the primary-α grains (Fig. 11(a)). These tend to act as the preferred initiation sites as the longest slip bands can form there, rather than in the secondary-α grains within the transformed β-matrix [53], and furthermore, many of the initiating primary-α grains are aligned with near-basal orientation perpendicular to the stress axis, as has been shown for this microstructure [54] using electron back scattered diffraction (EBSD) analysis (Fig. 11(b)). The shape of these small cracks, which is known to have a profound effect on their behavior [36,38,39], was assessed from observations of the subsequent fracture surfaces; this shape was taken to be semi-elliptical, with $a/2c$~0.45, and was assumed to remain constant with crack extension.

4.3.2. Small-crack thresholds

The variation in ΔG_{TH} thresholds with increasing mode-mixity for such small flaws is shown in Fig. 12, and compared with corresponding *worst case* data for both large and short fatigue cracks (Table 2). One such flaw, cycled at a phase angle of $\beta = 28°$, is shown in Fig. 13, together with the corresponding fracture surface associated with mixed-mode fatigue-crack growth under mixed-mode loading. Crack paths are normally the result of the interaction between the optimum crack-driving force and the nature of the local microstructure. Whereas for large and short cracks, the former was the dominant factor, it should be noted that the path followed by the small cracks was more strongly influenced by local microstructure.

The data shown in Fig. 12, which are believed to be the first reported results on mixed-mode fatigue thresholds for microstructurally-small cracks, were again determined from the average of the 'growth/no growth' conditions. In general, it can be seen that small-crack ΔG_{TH} thresholds vary little with mode-mixity; moreover, their values were lower than those obtained for short through-thickness cracks, and substantially lower than those for large through-thickness cracks. In terms of stress intensities, mixed-mode small crack $\Delta K_{eq,TH}$ thresholds are generally on the order of 1–2 MPa√m, compared to large-crack values between 3 and 10 MPa√m. Indeed, mixed-mode small-crack growth can be seen at driving forces below the established *worst case* large-crack threshold [8], and even below the 'shielding-corrected' large crack results. This is consistent with previous observations made on small surface cracks in this microstructure under pure mode I conditions, where ΔG_{TH} thresholds were found to be as low as 9.5 J/m^2 [54]. The origin of this effect is believed to be two-fold, as discussed below:

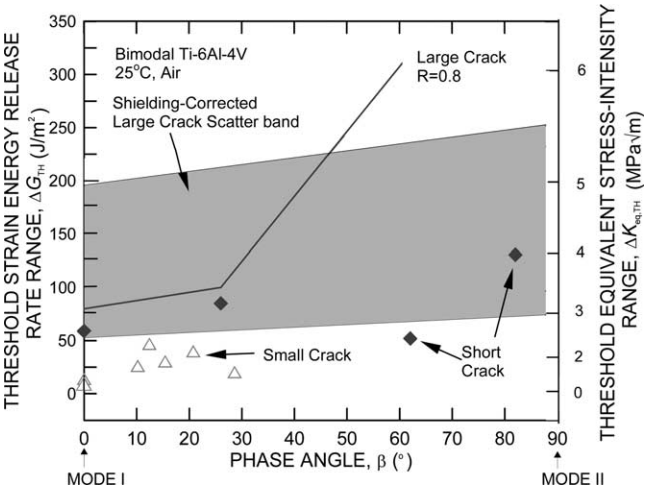

Fig. 12. Variation in mixed-mode thresholds, ΔG_{TH}, as a function of phase angle, β, for small (< 50 μm) surface cracks in the bimodal microstructure. Shown for comparison are results for short (~200 μm) through-thickness cracks and for large (> 4 mm) through-thickness cracks under *worst-case*, high *R* conditions.

Crack-tip shielding: As discussed above for short cracks, the highly restricted wake of the small cracks acts to severely limit any crack-tip shielding by crack closure and more importantly crack surface interference. Since the small crack ΔG_{TH} thresholds are comparable with the 'shielding-corrected' large crack values, it is reasonable to conclude that the limited effect of wake shielding accounts for the absence of an effect of mode-mixity on the small crack thresholds, and for their very small magnitude compared to corresponding (uncorrected) large-crack results. Similar behavior has been reported for pure mode I tests conducted previously in this bimodal Ti–6Al–4V [55]. However, of note here is the fact that the small crack thresholds are actually somewhat lower than the short crack and shielding-corrected large crack results, indicating that other factors are involved. One such factor involving microstructural sampling, is discussed below.

Microstructural sampling: As seen in Fig. 12, the correction for crack-tip shielding for microstructurally-small cracks does reduce the substantial difference between large and small crack thresholds; however, a significant discrepancy remains even after such corrections. This is believed to be the result of biased sampling of microstructural barriers by the crack front and local arrest at such barriers. Indeed, the ratio of crack size (or depth) to the average grain (microstructural unit) size will decide the exact microstructural environment that the crack-front interrogates. In the initial stages of growth, if the crack is small enough to be contained within a single grain, then the conditions experienced by the crack front are nominally similar to those experienced for growth within a single crystal, resulting in much higher growth rates (e.g. [56]). As the crack extends beyond the grain, the crack front samples more grains, with an increased probability of encountering unfavorably oriented features. However, a crack front with a length on the order of a few grain sizes does not always sample enough disadvantageously-oriented

Table 2
Approximate thresholds obtained for large, short and small fatigue cracks in Ti–6Al–4V

Mode mixity (deg)	ΔG_{TH}(J/m^2)			$\Delta K_{eq.TH}$(MPa$\sqrt{m}$)		
	R=0.1	R=0.5	R=0.8	R=0.1	R=0.5	R=0.8
Large cracks						
0	200	80	80	4.9	3.1	3.1
26	280	150	100	5.8	4.3	3.5
62	410	375	320	7.0	6.7	6.2
82	850	575	-	10.1	8.3	-
Short cracks						
0	72	66	59	2.9	2.8	2.7
26	125	105	85	3.9	3.6	3.2
62	72	64	52	2.9	2.8	2.5
82	148	140	130	4.2	4.1	4.0
Small cracks						
0	10	-	-	1.1	-	-
0	18	-	-	1.5	-	-
10.5	25	-	-	1.8	-	-
12.5	45	-	-	2.3	-	-
15.5	27	-	-	1.8	-	-
21	38	-	-	2.1	-	-
28	20	-	-	1.6	-	-

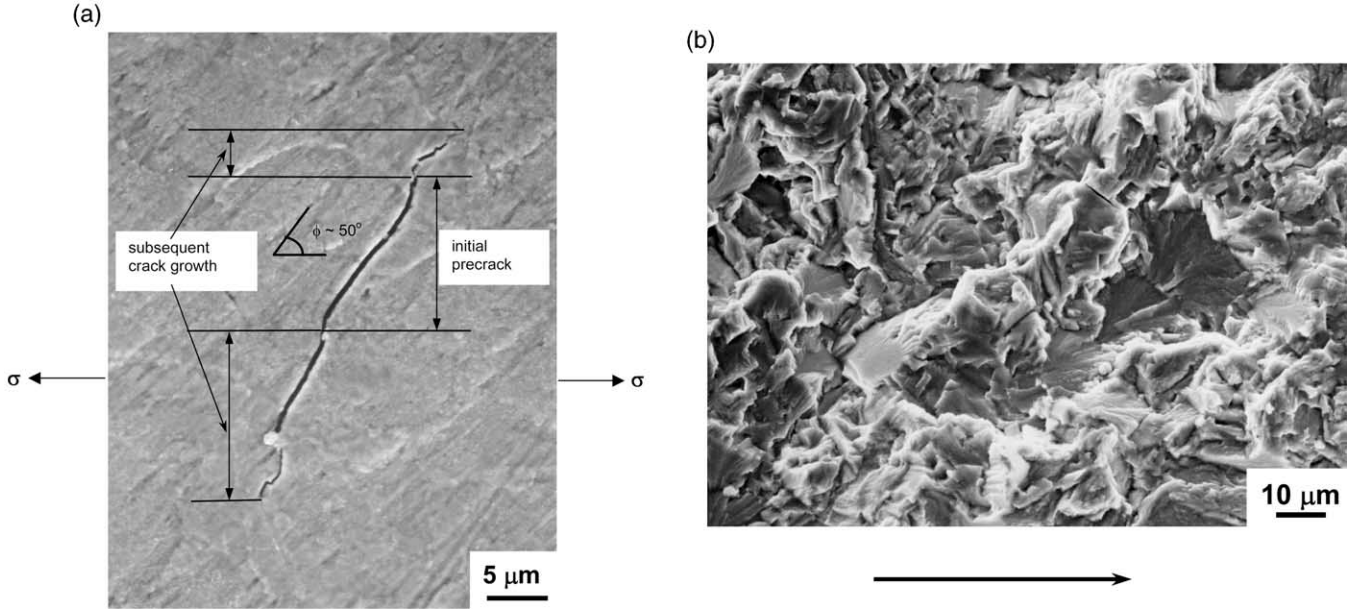

Fig. 13. (a) A typical crack path taken by a microstructurally-small crack under mixed-mode loading (R = 0.1, β ~ 28°, ΔG~20 J/m^2, angle of inclination ϕ~50°) is shown. The precrack was initiated under pure mode I; subsequent growth was under mixed-mode conditions. As is evident, there is a strong influence of local crack-tip microstructure on the crack path. (b) A typical fractograph for mixed-mode small crack growth (R = 0.1, β = 28°, ΔG~20 J/m^2). The arrow indicates the nominal direction of crack propagation.

grains to average out such effects. It has been suggested that this transition from microstructure-sensitive growth (seen for microstructurally-small cracks) to microstructure-insensitive growth (seen for large and short cracks) occurs when the crack size is roughly ten times the average grain size [57]. Since the small cracks investigated here were well below this limit (~200 μm), the measured crack propagation rates, and fatigue thresholds, were expected to be affected by microstructure, as was observed (Figs. 12–13). This is considered to be the prime reason for the lower ΔG_{TH} thresholds measured for such crack sizes.

5. Concluding remarks

In terms of the computed cyclic plastic-zone size in relation to crack size, all cracks examined in this study

can be considered to be linear elastic. Despite this, results clearly indicate a very significant effect of crack size on the mixed-mode fatigue thresholds, as summarized for the bimodal Ti–6Al–4V microstructure structure in Figs. 7, 9 and 12. Specifically, at a load ratio of 0.1, large-crack ΔG_{TH} mixed-mode thresholds at a near mode II mixity of $\Delta K_{II}/\Delta K_I \sim 7$ are some 70–90 times larger than measured short- and small-crack thresholds. Analogous to mode I behavior, this effect can be related to a restricted role of crack-tip shielding for the cracks with a limited wake and, where crack sizes approach microstructural dimensions, to biased sampling of the 'weak-links' in the microstructure by the small flaws. However, unlike mode I, the role of the crack-tip shielding, by mode I crack closure and more importantly mode II crack-surface interference, appears to be far more significant. For this reason, the difference in mixed-mode threshold values for cracks large and small compared to microstructural dimensions is far larger than is evident under pure mode I loading [54].

What is also apparent is that where crack sizes remain large with respect to microstructural dimensions, even though the loading is mixed-mode, the crack tends to follow a mode I ($K_{II} = 0$) path, an observation consistent with the fact that the measured ΔG_{TH} threshold is worst-case for pure mode I loading. Accordingly, from the perspective of design and 'lifing' methodologies for high-cycle fatigue, mode I ΔG_{TH} or ΔK_{TH} thresholds, (i) measured under extremely high load ratios [31], (ii) corrected for crack-tip shielding [21,22], or (iii) determined for short cracks (all procedures that minimize the effect of 'shielding'), can be used as a lower-bound for fatigue loading over the complete range of mode-mixities. However, where crack sizes approach microstructural dimensions, it is clear that they are not 'sampling' the continuum microstructure; as a consequence, continuum analyses such as deterministic fracture mechanics are only of limited utility and probabilistic methods need to be employed.

6. Conclusions

Mixed-mode (mode I+II) fatigue-crack growth thresholds for large (> 4 mm) and short (~200 μm) through-thickness cracks and microstructurally-small (< 50 μm) surface cracks have been examined in a fine-grained bimodal (STOA) microstructure (average grain size ~ 20 μm) of a Ti–6Al–4V turbine engine alloy over a range of load ratios from 0.1 to 0.8 and a range of mode-mixities from pure mode I, i.e. $\Delta K_{II}/\Delta K_I = 0$ (phase angle, $\beta = 0°$), to nearly pure mode II, i.e., $\Delta K_{II}/\Delta K_I \sim 7.1$ ($\beta = 82°$). Based on this work, the following observations can be made:

1. Fatigue thresholds for through-thickness cracks, large (> 4 mm) compared to microstructural dimensions, were found to be strongly influenced by load ratio and mode-mixity when measured under mixed-mode loading conditions.
2. Using the range of strain energy release rate, ΔG, incorporating both mode I and mode II contributions, as a single-parameter characterization of the crack-driving force, ΔG_{TH} thresholds values measured under pure mode I loading were found to be *worst case* for the range of mode-mixities studied. This was consistent with the fact that under mixed-mode loading, the initial extension of all cracks followed a mode I, i.e. a $K_{II} = 0$, path.
3. By experimentally measuring the magnitude of the crack-tip shielding, in the form of mode I crack closure and mode II crack-surface interference (by asperity rubbing and interlock), in order to estimate the effective (near-tip) mixed-mode driving force, ΔG_{eff}, 'shielding-corrected' mixed-mode thresholds were determined. Due to the significant influence of shielding under mixed-mode conditions, such $\Delta G_{TH,eff}$ threshold values were considerably lower than the 'uncorrected' ΔG_{TH} values, and showed minimal sensitivity to either load ratio and mode-mixity.
4. These observations strongly imply that for cracks large compared to microstructural dimensions, fatigue cracking under mixed-mode loading is predominately a mode I phenomenon. The significant influence of mode-mixity (and load ratio) on measured mixed-mode thresholds can be attributed primarily to crack-tip shielding, in particular from crack-surface interference.
5. This is consistent with observations of the corresponding mixed-mode ΔG_{TH} thresholds for short (~200 μm) through-thickness cracks, obtained by machining off the wake of large cracks. The magnitude of such short-crack thresholds was significantly lower than those measured for large cracks, and was found to be comparable with the crack-tip shielding-corrected large-crack thresholds. Moreover, they were essentially independent of mode-mixity and load ratio, again suggesting a predominant role of shielding on mixed-mode fatigue threshold behavior.
6. Corresponding mixed-mode fatigue threshold results for microstructurally-small (< 50 μm) surface cracks indicated that this marked reduction in ΔG_{TH} thresholds with diminishing crack dimensions may be even greater when crack sizes approach the scale of microstructure. This was rationalized in terms of the 'biased' sampling the microstructure by such small flaws, in addition to a reduced contribution of crack-tip shielding from their limited crack wake.

Acknowledgements

This work was supported by the US Air Force Office of Scientific Research under Grant No. F49620-96-1-0478 under the auspices of the Multidisciplinary University Research Initiative on High Cycle Fatigue to the University of California at Berkeley. Special thanks are due to Drs. B.L. Boyce, I. Altenberger, J.O. Peters and A.W. Thompson for helpful discussions.

Appendix A

Distinction between large, short and small cracks

For the sake of clarity, the salient differences between *large*, *short* and *small* cracks are summarized. Large fatigue cracks [Fig. 14(a)] have fracture surface dimensions that are large compared to the scale of the microstructure in both directions. They therefore generally have a fully developed[5] crack-tip shielding zone and can 'sample' the microstructure in a statistical (continuum) manner [23]. With respect to large cracks, small cracks are generally described as being comparable in size to [24]:

- microstructural dimensions, where biased statistical sampling of the microstructure can lead to accelerated crack advance along 'weak' paths, i.e., microstructural features oriented for easy crack growth (a continuum limitation),
- the extent of local inelasticity *ahead* of the crack tip, where the assumption of small-scale yielding implicit in the use of the stress intensity, *K*, is not strictly valid (a linear-elastic fracture mechanics limitation),
- the extent of crack-tip shielding (e.g., crack closure) *behind* the crack tip, where the reduced role of shielding leads to a higher local driving force than the corresponding large crack at the same applied *K* level (a similitude limitation).

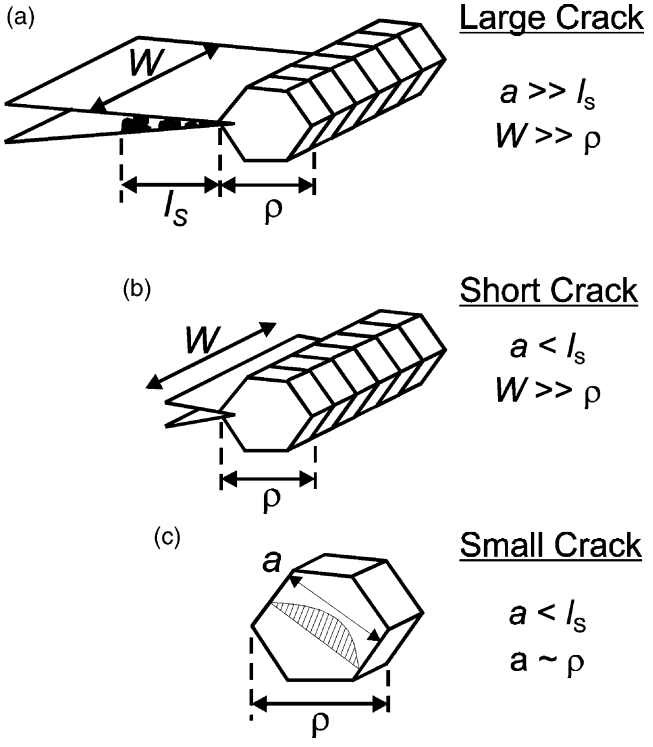

Fig. 14. Schematic illustrations highlighting the key distinctions between large, short and small fatigue cracks. Large cracks (a) have length, a, and width, W, which are large both with respect to the equilibrium shielding-zone length, ls (indicated here as a region of debris in the crack wake which produces crack closure), and the characteristic microstructural size scale, r, e.g., the grain size. In contrast to this, short fatigue cracks (b) are characterized by a $<$ ls, but $W \gg \rho$. The reduced crack-wake length results in a lower level of crack-tip shielding. For small cracks (c), the fracture surface is reduced in both dimensions, with a (and W) being small with respect to both ls and r. The fact that $a \sim \rho$ implies that the crack front samples only a few microstructural entities, leading to a biased sampling of the microstructure.

However, a further distinction can be made between short and small cracks (Fig. 14). This distinction alludes not simply to physical size but the extent to which a fatigue crack is subjected to the first and third factors listed above. Short fatigue cracks (Fig. 14(b)) are physically short in only one dimension, a condition that is often realized experimentally by machining away the wake of a large crack. This type of fatigue flaw experiences limited crack-tip shielding due to its reduced length [25], yet still samples the microstructure as a continuum because of its extensive crack front. In contrast, small fatigue cracks (Fig. 14(c)) are small and comparable to the microstructural size scale in all dimensions, as typified by the small, semi-elliptical surface flaw (e.g. [24]). With such cracks, crack-tip shielding is significantly reduced (e.g. [23]), and since the crack front samples only few microstructural entities, this allows for a biased sampling of microstructurally weak paths. Because of this restriction in shielding and the biased microstructural sampling, fatigue-crack growth resistance in the presence of small cracks tends to be lowest.

[5] For mixed-mode loading conditions, the shearing of the fracture surfaces with respect to one another can produce crack-wake contact via sliding interference over dimensions which are much larger than for mode I loading, perhaps over the entire wake of a large fatigue crack (e.g., [45–47]). Thus, the notion of a 'fully developed' shielding zone is somewhat unclear for mixed-mode loading conditions. At the least, one would expect the equilibrium shielding-zone length to be a function of the applied ratio of shear to tension.

Appendix B

Calculation of the mixed-mode threshold

In this work, as in prior studies (e.g. [16-18,21,22,42]) on mixed-mode fatigue thresholds, the threshold values of the mode I and mode II stress intensities required to initiate cracking, $\Delta K_{I,TH}$ and $\Delta K_{II,TH}$, are calculated based on the mode I precrack (which is generated in near-identical fashion for each test); the corresponding mixed-mode threshold, ΔG_{th}, or equivalent stress intensity, $\Delta K_{eq,TH}$, are then computed from:

$$\Delta G_{TH} = (\Delta K_{I,TH}^2 + \Delta K_{II,TH}^2)/E' \equiv (\Delta K_{eq,TH}^2)/E', \quad \text{(B1)}$$

where E' is the appropriate elastic modulus.

However, once the crack starts to grow, it deflects along a different path (generally corresponding to a local $K_{II} = 0$ criterion modified by the effect of the microstructure). Consequently, an alternative calculation of the threshold can be based on the presence of an infinitesimal kink along this direction. Assuming for simplicity that the kink (of length $b << a$, the crack length) represents an in-plane tilt through angle α to the precrack plane (Fig. 15), then the local mode I and mode II stress intensities, Δk_1 and Δk_2, at the deflected crack tip will be given by [58,59]:

$$\Delta k_1(\alpha) = c_{11}\Delta K_1 + c_{12}\Delta K_{II}$$
$$\Delta k_2(\alpha) = c_{21}\Delta K_1 + c_{22}\Delta K_{II}. \quad \text{(B2)}$$

where ΔK_I and ΔK_{II} are the stress intensities for a main (pre)crack, and the coefficients c_{ij}, which are a sole function of α, are given in [58,59]. The mixed-mode thresholds, $\Delta G'_{TH}$ and $\Delta K'_{eq,TH}$, can then computed from:

$$\Delta G'_{TH} = (\Delta k_{1,TH}^2 + \Delta k_{2,TH}^2)/E' \equiv (\Delta K'^2_{eq,TH})/E'. \quad \text{(B3)}$$

For the present results, the use of (B3) can either increase or decrease the mixed-mode threshold, as shown for both large and short cracks in Fig. 16. In general though, the trend is to reduce the computed values of $\Delta K_{eq,TH}$ somewhat, except at very high phase angles. At $\beta = 26°$, however, the large crack $\Delta K_{eq,TH}$ threshold is reduced by as much as 40%; for the bimodal Ti–6Al–4V, this translates into a reduction in threshold $\Delta K_{eq,TH}$ values by between 1 and 2 MPa√m. Effects are far less significant for the short cracks.

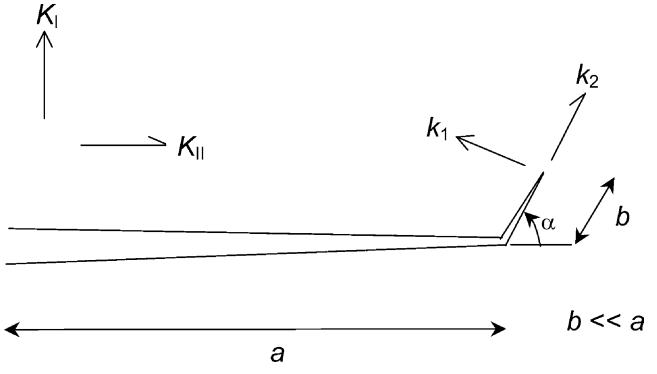

Fig. 15. Schematic illustration of the kinked crack configuration for the alternative calculation of the mixed-mode threshold.

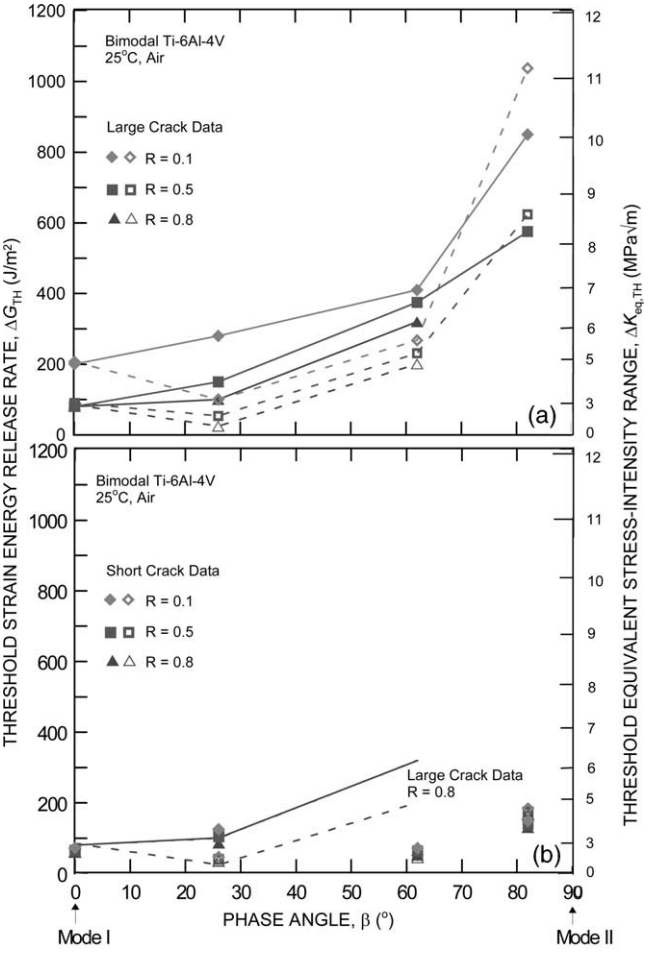

Fig. 16. (a) Mixed mode thresholds for (a) large cracks and (b) short cracks, calculated using the single-parameter characterization [21-22] (solid lines, solid data points) and using the kink-based calculations (dotted lines, hollow data points).

References

[1] Report of the AdHoc Committee on Air Force Aircraft Jet Engine Manufacturing and Production Processes, United States Air Force Scientific Advisory Board, SAF/AQQS: the Pentagon, Washington, DC,1992.
[2] Chang JCI. An integrated research approach to attack engine HCF problems. Air Force Office of Scientific Research, Bolling AFB, Washington, DC; 1996.
[3] Cowles BA. High cycle fatigue in aircraft gas turbines—an industry perspective. Int J Fract 1996;80:147–63.
[4] Waterhouse RB, Lindley TC, editors. Fretting fatigue, European

Structural Integrity Society publication no. 18. London: Mechanical Engineering Publications Ltd; 1994.
[5] Irwing PE, Beevers CJ. The effect of air and vacuum environments on fatigue crack growth rates in Ti-6Al-4V. Metall Trans 1974;5:391–8.
[6] Bache MR, Evans WJ, McElhone MT. The effects of environment and internal oxygen on fatigue crack propagation in Ti-6Al-4V. Mater Sci Eng A 1997;234-236:918–22.
[7] Thomas JP. Subcritical crack growth of Ti-6Al-4V at room temperature under high stress-ratio loading. Scripta Mater 1998;39:1647–52.
[8] Ritchie RO, Boyce BL, Campbell JP, Roder O, Thompson AW, Milligan WW. Thresholds for high-cycle fatigue in a turbine engine Ti-6Al-4V alloy. Int J Fat 1999;21:653–62.
[9] Wanhill RJH. Environmental fatigue crack propagation in Ti-6Al-4V sheet. Metall Trans A 1976;7:1365–73.
[10] Iida S, Kobayashi AS. Crack-propagation rate in 7075-T6 plates under cyclic tensile and transverse shear loadings. J Basic Eng 1969;91:764–9.
[11] Abdel-Mageed AM, Pandey RK. Mixed mode crack growth under static and cyclic loading in Al-alloy sheets. Eng Fract Mech 1991;40:371–85.
[12] Tschegg EK, Stanzl SE, Czegley M. Crack face interactions and near-threshold fatigue crack growth. Fat Fract Eng Mater Struct 1993;16:71–83.
[13] Hua G, Brown MW, Miller KJ. Mixed-mode fatigue thresholds. Fat Fract Eng Mater Struct 1982;51:1–17.
[14] Tong J, Yates JR, Brown MW. The significance of mean stress on the fatigue crack growth threshold for mixed mode I+II loading. Fat Fract Eng Mater Struct 1994;17:829–38.
[15] Qian J, Fatemi A. Mixed mode fatigue crack growth: a literature survey. Eng Fract Mech 1996;55:969–90.
[16] Pustejovsky MA. Fatigue crack propagation in titanium under general in-plane loading. 1. Experiments. Eng Fract Mech 1979;11:9–15.
[17] Pustejovsky MA. Fatigue crack propagation in titanium under general in-plane loading. II. Analysis. Eng Fract Mech 1979;11:17–31.
[18] Gao H, Alagok N, Brown MW, Miller KJ. Growth of fatigue cracks under combined mode I and mode II loads. In: Miller KJ, Brown MW, editors. Multiaxial fatigue, ASTM STP 853. Philadelphia, PA: American Society for Testing and Materials; 1985. p. 184–202.
[19] Taylor D. A compendium of fatigue thresholds and crack growth rates. Warley (UK): EMAS Ltd, 1985.
[20] Ritchie RO. Small cracks and high-cycle fatigue. In: Chang JCI, Coulter J, Brei D, Martinez D, Hg W, Freidmann PP, editors. Proceedings of the ASME Aerospace Division, AMD. New York: ASME; 1996. p. 321–33.
[21] Campbell JP, Ritchie RO. Mixed-mode, high-cycle fatigue-crack growth thresholds in Ti-6Al-4V. I. A comparison of large- and short-crack behavior. Eng Fract Mech 2000;67:209–27.
[22] Campbell JP, Ritchie RO. Mixed-mode, high-cycle fatigue-crack growth thresholds in Ti-6Al-4V II: Quantification of crack-tip shielding. Eng Fract Mech 2000;67:229–49.
[23] Suresh S, Ritchie RO. Propagation of short cracks. Int Metals Rev 1984;29:445–76.
[24] Ritchie RO, Lankford J. Small fatigue cracks: a statement of the problem and potential solutions. Mater Sci Eng A 1986;84:11–6.
[25] Ritchie RO, Wu Y. Short crack effects in fatigue: a consequence of crack tip shielding. In: Ritchie RO, Lankford J, editors. Small fatigue cracks. Warrendale, PA: TMS-AIME; 1986. p. 167–89.
[26] Venkateswara Rao KT, Yu W, Ritchie RO. On the behavior of small fatigue cracks in commercial aluminum-lithium alloys. Eng Fract Mech 1988;31:623–35.
[27] Boyce BL. M.S. thesis, University of California at Berkeley, 1998.
[28] Eylon D. Summary of available information on the processing of the Ti-6Al-4V HCF/LCF program plates, University of Dayton report, Dayton, OH, 1998.
[29] Suresh S, Shih CF, Morrone A, O'Dowd NP. Mixed-mode fracture toughness of ceramic materials. J Am Ceram Soc 1990;73:1257–67.
[30] He MY, Hutchinson JW. Asymmetric four-point crack specimen. J Appl Mech Trans ASME 2000;67:207–9.
[31] Boyce BL, Ritchie RO. Effect of load ratio and maximum stress intensity on the fatigue threshold in Ti-6Al-4V. Eng Fract Mech 2001;68:129–47.
[32] Dowling NE. Notched member fatigue life predictions combining crack initiation and propagation. Fat Eng Mater Struct 1979;2:129–38.
[33] Hammouda MM, Smith RA, Miller KJ. Elastic-plastic fracture mechanics for initiation and propagation of notch fatigue cracks. Fat Eng Mater Struct 1979;2:139–54.
[34] Rice JR, Johnson MA. The role of large crack geometry changes in plane strain fracture. In: Kanninen MF, Adler WG, Rosenfield AR, Jaffee RI, editors. Inelastic behavior of solids. New York: McGraw-Hill; 1970. p. 641–72.
[35] Hill R. The mathematical theory of plasticity. Oxford: Clarendon Press, 1950.
[36] Newman JC, Raju IS. An empirical stress-intensity factor equation for the surface crack. Eng Fract Mech 1981;15:185–92.
[37] He MY, Hutchinson JW. Surface crack subject to mixed mode loading. Eng Fract Mech 2000;65:1–14.
[38] Ravichandran KS. Effects of crack aspect ratio on the behavior of small surface cracks in fatigue: Part I. Simulation. Metall Mater Trans A 1997;28:149–56.
[39] Ravichandran KS, Larsen JM. Effects of crack aspect ratio on the behavior of small surface cracks in fatigue: Part II. Experiments on a titanium (Ti-8Al) alloy. Metall Mater Trans A 1997;28:157–69.
[40] Zheng YS, Wang ZG, Ai SH. Mixed-mode I and II fatigue threshold and crack closure in dual-phase steels. Metall Mater Trans A 1994;25:1713–23.
[41] Yao D, Shang JK. Effect of load mix on fatigue crack growth in 63Sn-37Pb solder joints. J Elect Pack Trans ASME 1997;119:114–8.
[42] Campbell JP, Ritchie RO. Mixed-mode, high-cycle fatigue-crack-growth thresholds in Ti-6Al-4V: role of bimodal and lamellar microstructures. Metall Mater Trans A 2001;32:497–503.
[43] Erdogan F, Sih GC. On the crack extension in plates under plane loading and transverse shear. J Basic Eng Trans ASME 1963;85:519–25.
[44] Pook LP. The fatigue crack direction and threshold behavior of mild steel under mixed modes I and III. Int J Fat 1985;7:21–30.
[45] Nayeb-Hashemi H, McClintock FA, Ritchie RO. Effects of friction and high torque on fatigue crack propagation in Mode III. Metall Trans A 1982;13:2197–204.
[46] Tschegg EK, Ritchie RO, McClintock FA. On the influence of rubbing fracture surfaces on fatigue crack propagation in mode III. Int J Fat 1983;5:29–35.
[47] Tschegg EK. Sliding mode crack closure and mode III fatigue crack growth in mild steel. Acta Metall 1983;31:1323–30.
[48] Gao H, de los Rios ER, Miller KJ. Mixed-mode fracture mechanisms near the fatigue threshold of AISI 316 stainless steel. Fat Eng Mater Struct 1983;6:137–47.
[49] Tong J, Yates JR, Brown MW. A model for sliding mode crack closure. I. Theory for pure mode II loading. Eng Fract Mech 1995;52:599–611.
[50] Tong J, Yates JR, Brown MW. A model for sliding mode crack closure. II. Mixed mode I and II loading and application. Eng Fract Mech 1995;52:613–23.
[51] Ritchie RO. Mechanisms of fatigue crack propagation in metals,

ceramics and composites: role of crack-tip shielding. Mater Sci Eng 1988;103:15–28.
[52] Ritchie RO. Mechanisms of fatigue-crack propagation in ductile and brittle solids. Int J Fract 1999;100:53–83.
[53] Thompson AW. Relations between microstructure and fatigue properties of alpha-beta titanium alloys. In: Boyer RR, Eylon D, Lütjering G, editors. Fatigue behavior of titanium alloys. Warrendale, PA: TMS; 1999. p. 23–30.
[54] Peters JO, Boyce BL, Chen X, McNaney JM, Hutchinson JW, Ritchie RO. On the application of the Kitagawa-Takahashi diagram to foreign-object damage and high-cycle fatigue. Eng Fract Mech, in press.
[55] Nalla RK, Boyce BL, Campbell JP, Peters JO, Ritchie RO. Influence of microstructure on high-cycle fatigue of Ti-6Al-4V: bimodal vs. lamellar structures. Metall Mater Trans A 2002;33A:899–918.
[56] Lankford J, Davidson DL. The role of metallurgical factors in controlling the growth of small fatigue cracks. In: Ritchie RO, Lankford J, editors. Small fatigue cracks. Warrendale, PA: TMS; 1986. p. 51–71.
[57] Taylor D, Knott JF. Fatigue crack propagation behavior of short cracks: the effect of microstructure. Fat Eng Mater Struct 1981;4:147–55.
[58] Bilby BA, Cardew GE, Howard IC. Stress intensity factors at the tips of kinked and forked cracks. In: Taplin DMR, editor. Fracture 1977. Oxford: Pergamon Press; 1977. p. 197–200.
[59] Cotterell B, Rice JR. Slightly curved or kinked cracks. Int J Fract 1980;16:155–69.